A Unified Instance Segmentation Framework for Completely Occluded Objects and Dense Objects in Robot Vision Measurement

Zhen Zhou[1,2], Junfeng Fan[1], Yunkai Ma[1,2], Sihan Zhao[1,2], Fengshui Jing[1,2,*], Min Tan[1,2]

Abstract— Instance segmentation for completely occluded objects and dense objects in robot vision measurement are two challenging tasks. To uniformly deal with them, this paper proposes a unified coarse-to-fine instance segmentation framework, CFNet, which uses box prompt-based segmentation foundation models (BSMs), e.g., Segment Anything Model. Specifically, CFNet first detects oriented bounding boxes (OBBs) to distinguish instances and provide coarse localization information. Then, it predicts OBB prompt-related masks for fine segmentation. CFNet performs instance segmentation with OBBs that only contain partial object boundaries on occluders to predict occluded object instances, which overcomes the difficulty of existing amodal instance segmentation methods in directly predicting occluded objects. In addition, since OBBs only serve as prompts, CFNet alleviates the over-dependence on bounding box detection performance of current instance segmentation methods using OBBs for dense objects. Moreover, to enable BSMs to handle OBB prompts, we propose a novel OBB prompt encoder. To make CFNet more lightweight, we perform knowledge distillation on it and introduce a Gaussian label smoothing method for teacher model outputs. Experiments demonstrate that CFNet outperforms current instance segmentation methods on both industrial and public datasets. The code is available at https://github.com/zhen6618/OBBInstanceSegmentation.

I. INTRODUCTION

Instance segmentation provides foundational information for numerous tasks based on robot vision measurement, such as robot grasping [1], [2] and autonomous driving [3]. This work focuses on two challenging difficulties in robot vision measurement: completely occluded object instance segmentation and dense object instance segmentation. We aim to develop a unified framework to handle these difficulties.

Instance segmentation for completely occluded objects (called occludees) is difficult, since the information available for inferring occluded objects is very limited. For example, in Fig. 1(a), instance segmentation of reference holes that provide optimal assembly positions is usually required in robot assembly tasks. In several scenarios, reference holes (i.e., occludees) are screwed with bolts and nuts, completely occluded by these industrial parts (called occluders). To perform instance segmentation on occludees, current amodal instance segmentation methods [4]–[7] directly predict occludees. Although they can automatically extract features
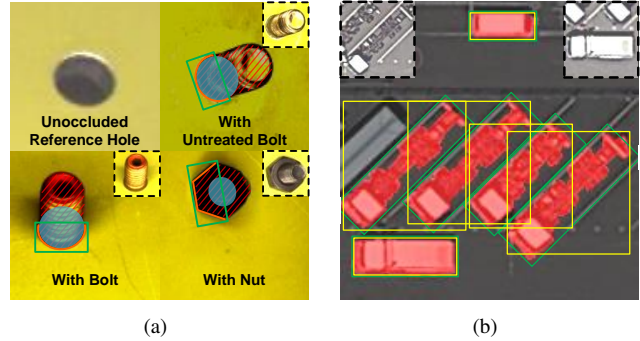
Fig. 1. Examples of completely occluded objects (a) and dense objects (b). Original objects are inside the corresponding black dotted boxes. (a): reference holes (blue) are occluded by bolts or nuts (i.e., occluders, shown in red). Oriented bounding boxes (green) contain occluder boundaries (orange) that are located at the contact surface between occluders and occluded reference holes. (b): dense vehicles (red) are surrounded by horizontal bounding boxes (yellow) or oriented bounding boxes (green).

related to occludees for inference, the performance is poor.

Dense object instance segmentation is a long-standing challenge [8] in robot vision measurement. For instance, in Fig. 1(b), objects are densely packed in multiple orientations in unmanned aerial vehicle (UAV) measurement. Since horizontal bounding boxes (HBBs) introduce many interference areas, oriented bounding boxes (OBBs) are often used for instance identification [9]–[12], e.g., ISOP [12] predicts masks in the detected OBBs. However, bounding box-based instance segmentation methods are overly dependent on bounding box detection performance, especially for OBBs that are sensitive to both position and orientation. This dependence makes instance segmentation methods using OBBs more difficult and unstable.

In this paper, we propose CFNet, a unified coarse-to-fine framework for both completely occluded and dense object instance segmentation, which uses box prompt-based segmentation foundation models (BSMs), e.g., Segment Anything Model (SAM) [13]. CFNet first detects OBBs to distinguish instances, identify classes, and provide coarse localization information. Then, it predicts OBB-related segmentation masks. Our motivation is inspired by the powerful segmentation capabilities of BSMs and their excellent box prompt mechanisms. CFNet uses an OBB detection module (e.g., Oriented R-CNN [14]) for coarse detection, and leverages BSMs to predict OBB-related masks for fine segmentation.

CFNet improves BSMs in two aspects. First, to handle OBB prompts, CFNet introduces a novel OBB prompt encoder. Second, since BSMs usually have high computational

complexity, we perform knowledge distillation on the box prompt encoders and mask decoders. Specifically, a Gaussian smoothing method for teacher model outputs is introduced. In this work, CFNet chooses SAM as the baseline model and makes improvements in the above two aspects.

Compared with amodal instance segmentation methods, CFNet avoids directly predicting occludee instances by performing instance segmentation with OBBs that only contain partial object boundaries on occluders to infer occludees. In addition, OBBs used in CFNet provide more accurate location information than HBBs used in amodal instance segmentation methods. Compared with current instance segmentation methods using OBBs for dense objects, CFNet only uses OBBs as prompts to guide object segmentation, so the segmentation results are less dependent on bounding box detection performance, which improves instance segmentation performance. Moreover, CFNet is based on BSMs that are pretrained on large-scale data for segmentation tasks, helping to enhance feature extraction and segmentation capabilities. The main contributions are summarized as follows.

- We propose CFNet, a unified coarse-to-fine framework for both completely occluded and dense object instance segmentation in robot vision measurement. CFNet uses BSMs and outperforms current instance segmentation methods on both industrial and public datasets.
- A novel OBB prompt encoder is proposed to effectively encode OBB prompts and guide BSMs to generate OBB prompt-related segmentation masks.
- We propose a knowledge distillation method for the OBB prompt encoders and mask decoders of BSMs, significantly reducing the computational complexity with a minor loss in accuracy. Specifically, a Gaussian smoothing method for teacher model outputs is proposed.

II. RELATED WORK

A. Amodal Instance Segmentation

Amodal instance segmentation directly predicts completely occluded object instances. The first amodal instance segmentation method [7] predicted the amodal masks and corresponding bounding boxes in an iterative bounding box expansion manner. Zhu et al. [15] directly trained general instance segmentation methods on amodal instance segmentation datasets. Based on Mask R-CNN [16], Qi et al. [5] predicted occluded parts by adding a multi-task branch with multi-level coding. Similarly, based on Mask R-CNN, ORCNN [6] first predicted amodal masks through an amodal mask prediction branch and then combined a visible mask prediction branch to predict occluded parts. Different from the above methods that only considered occludees, BCNet [4] proposed a bilayer graph convolutional network to simultaneously consider interactions between occluders and occludees. Since the information available for inferring occludees is very limited, these methods have poor performance.

B. Instance Segmentation with Oriented Bounding Boxes

Compared with instance segmentation with HBBs [16], [17], instance segmentation with OBBs that have less inter-

ference areas provides more accurate location information. Based on Mask R-CNN, a Region of Interest (RoI) learner was applied to HBB proposals to generate OBB proposals, followed by a head that generated segmentation masks [12]. Based on a similar idea, Feng et al. [11] proposed a part-aware instance segmentation network with OBB proposals for bin picking. Follmann and König [10] first generated the final OBBs using a two-stage object detection approach, and then predicted masks within the detected OBBs. Rotated Blend Mask R-CNN [9] proposed a top-down and bottom-up structure for oriented instance segmentation. However, these methods are overly dependent on OBB detection performance, making predictions more difficult and unstable.

C. Box Prompt-Based Segmentation Foundation Models

Benefiting from pretraining on large-scale data for segmentation tasks, BSMs exhibit powerful segmentation and generalization capabilities. For example, SAM [13] was trained on more than 1B segmentation masks from 11M images, showing remarkable segmentation and zero-shot generalization capabilities. A BSM for medical image segmentation is proposed in [18]. To enhance interactive performance, BSMs incorporate prompt mechanisms. A representative work is SAM, which took HBBs as prompts and predicted segmentation masks with respect to HBBs. MobileSAM [19] retained the HBB prompt mechanism and proposed a lightweight version of SAM for edge devices.

D. Box Prompt Encoder

Existing methods usually use HBBs as box prompts for BSMs, such as SAM and MobileSAM. The current designs of HBB prompt encoders are mainly inspired by SAM. A HBB was represented by two points, i.e., the top-left corner point and the bottom-right corner point. Then, a point was encoded as the sum of a Gaussian positional encoding [20] of the location and a learned embedding representing the top-left corner or bottom-right corner. Hence, a box was encoded as a combination of the two encoded point embeddings. However, to the best of our knowledge, there is no relevant research on OBB prompt encoders yet.

E. Label Smoothing for Box Prompt encoders and Segmentation networks in Knowledge Distillation

In knowledge distillation for segmentation tasks, label smoothing helps reduce overfitting and enhances model performance. Inception-v3 [21] proposed uniform label smoothing (ULS), i.e., the weighted average of one-hot labels and uniform distributions. Spatially varying label smoothing (SVLS) [22] applied a discrete spatial Gaussian kernel to segmentation labels to smooth one-hot labels. These two label smoothing methods were commonly used in segmentation tasks. For example, Park et al. [23] applied ULS and proposed pixel-wise adaptive label smoothing for self-distillation. P-CD [24] utilized SVLS to generate segmentation boundary uncertainty and soft targets. Unlike applying SVLS to ground truth (GT) labels, we apply Gaussian smoothing to the segmentation masks of the teacher model,
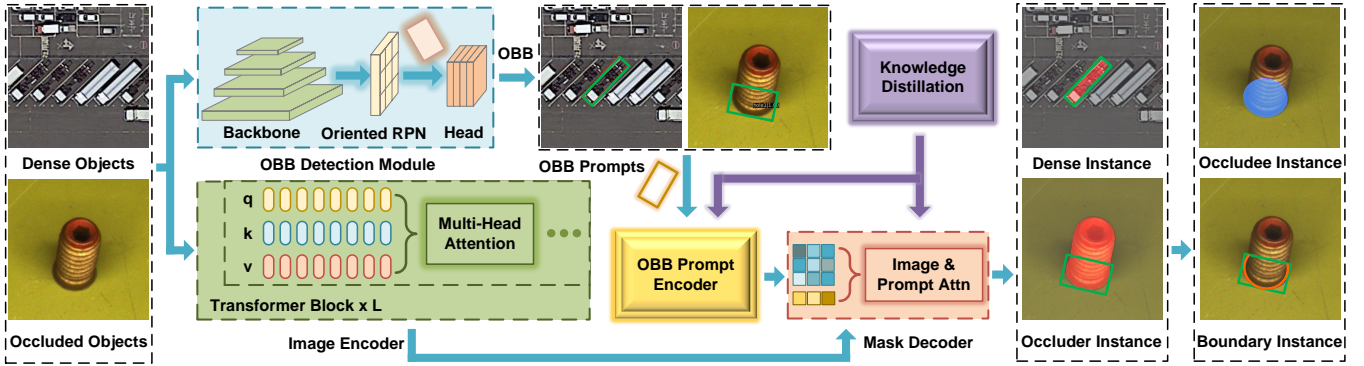
Fig. 2. Architecture of the proposed CFNet. Compared with dense object instance segmentation, completely occluded object instance segmentation needs more post-processing steps to transform occluder instances into occludee instances.

which yields better distillation performance. As for label smoothing methods used for box prompt encoders, to our knowledge, no relevant research has been published yet.

III. METHODS

A. Overview

The structure of CFNet is shown in Fig. 2. It is mainly composed of four parts: an OBB detection module, an image encoder, an OBB prompt encoder, and a mask decoder. Specifically, images containing dense or occluded objects serve as input. The OBB detection module is used to detect OBBs that distinguish instances, identify classes, and provide coarse localization information. The image encoder is used to transform input images into high-dimensional feature representations and generate image embeddings. The OBB prompt encoder is responsible for encoding OBB prompts and generating prompt embeddings. Then, the image embeddings and prompt embeddings are combined in the mask decoder to predict OBB prompt-related segmentation masks.

For dense object instance segmentation, CFNet detects OBBs that encompass entire instances and predicts segmentation masks of dense objects. For completely occluded object instance segmentation, CFNet avoids directly predicting occludee instances by performing instance segmentation with OBBs that only contain partial object boundaries on occluders. Specifically, OBBs contain occluder boundaries that are located at the contact surface between occluders and occludees (see Fig. 1(a)). Then, post-processing steps transform occluder instances into partial boundary instances and use prior geometric relationships between boundary instances and occludee instances to obtain occludee instances (e.g., in robot assembly, the boundary shape of the occluded reference holes is an ellipse). However, partial bounding boxes are not suitable for current instance segmentation methods since their bounding boxes are usually designed to encompass entire instances.

Furthermore, knowledge distillation is applied to the OBB prompt encoder and mask decoder to reduce the computational complexity and make CFNet more lightweight. For OBB detection, we directly employ Oriented R-CNN [14], which is a two-stage OBB detection model with competitive detection accuracy and inference speed.

B. Oriented Bounding Box Prompt Encoder

The flowchart of the proposed OBB prompt encoder is described in Fig. 3. The detected OBBs are generated by the OBB detection module. An OBB is first parameterized as $(x_1, y_1, x_2, y_2, \sin\theta, \cos\theta)$, where (x_1, y_1), (x_2, y_2) and $(\sin\theta, \cos\theta)$ represent the top-left corner point, bottom-right corner point and orientation, respectively. We further denote

$$\varphi_1 = (x_1, y_1), \quad \varphi_2 = (x_2, y_2), \quad \boldsymbol{\theta} = (\sin\theta, \cos\theta),$$
$$\varphi_1 \in [0,1)^2, \quad \varphi_2 \in [0,1)^2, \quad \boldsymbol{\theta} \in [0,1)^2, \quad (1)$$

where (φ_1, φ_2) and $\boldsymbol{\theta}$ are normalized pixel coordinates and normalized orientation coordinates, respectively. Considering the difference between position information (φ_1, φ_2) and orientation information $(\boldsymbol{\theta})$, we first encode them separately and then fuse their encoded features.

Coordinate-based multilayer perceptrons (MLPs) take low-dimensional coordinates as input, such as φ_1, φ_2 and $\boldsymbol{\theta}$, and they have difficulty learning high-frequency information [20]. In CFNet, there are many MLP structures and transformer structures containing MLPs, so such a problem will degrade instance segmentation performance. To alleviate this problem, inspired by Gaussian positional encoding (GPE) for coordinates [20], CFNet introduces adaptive GPE (AGPE) to map the coordinate set $(\varphi_1, \varphi_2, \boldsymbol{\theta})$ into random Fourier features to better learn high-frequency information and enhance the performance of coordinate-based MLPs.

Given a d-dimensional coordinate $\boldsymbol{\tau} \in [0,1)^d$, the dense Fourier feature mapping is

$$\gamma(\boldsymbol{\tau}) = [a_0 \cos(2\pi \boldsymbol{G}_0^T \boldsymbol{\tau}), b_0 \sin(2\pi \boldsymbol{G}_0^T \boldsymbol{\tau}), \dots$$
$$a_i \cos(2\pi \boldsymbol{G}_i^T \boldsymbol{\tau}), b_i \sin(2\pi \boldsymbol{G}_i^T \boldsymbol{\tau}), \dots]^T, \quad (2)$$

where a_i and b_i $(i = 0, \dots, \infty)$ are Fourier series coefficients, and $\boldsymbol{G}_i \in \mathbb{R}^d$ is the corresponding Fourier basis frequency. Since random sparse sampling of Fourier features through an MLP matches the performance of using a dense sampling of Fourier features with the same MLP [20], AGPE sets all a_i and b_i to 1. $\boldsymbol{G}_i$ is sampled from a Gaussian
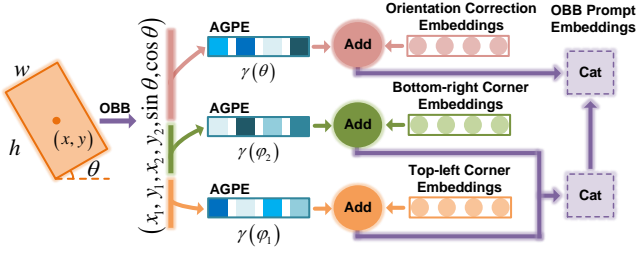
Fig. 3. Architecture of the proposed OBB prompt encoder. The input is an OBB (x, y, w, h, θ), where (x, y), w, h and θ represent the center point, width, height and orientation, respectively.
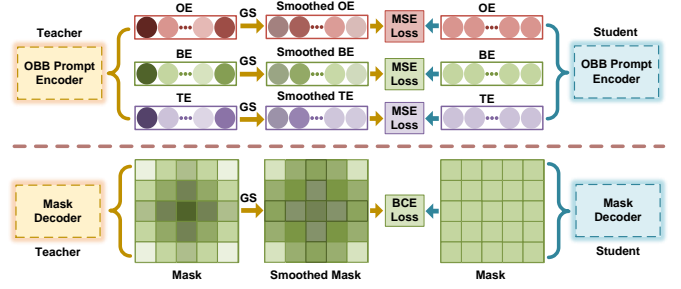

Fig. 4. The process of knowledge distillation for the OBB prompt encoder and mask decoder. "TE", "BE" and "OE" represent encoded feature embeddings with respect to the top-left point, bottom-right point and orientation of an OBB, respectively. "GS" stands for Gaussian smoothing.

distribution. Hence, the mapped random Fourier features are

$$\gamma(\boldsymbol{\varphi}_1) = [\cos(2\pi G_{\boldsymbol{\varphi}_1}\boldsymbol{\varphi}_1), \sin(2\pi G_{\boldsymbol{\varphi}_1}\boldsymbol{\varphi}_1)]^T, \qquad (3)$$

$$\gamma(\boldsymbol{\varphi}_2) = [\cos(2\pi G_{\boldsymbol{\varphi}_2}\boldsymbol{\varphi}_2), \sin(2\pi G_{\boldsymbol{\varphi}_2}\boldsymbol{\varphi}_2)]^T, \qquad (4)$$

$$\gamma(\boldsymbol{\theta}) = [\cos(2\pi G_{\boldsymbol{\theta}}\boldsymbol{\theta}), \sin(2\pi G_{\boldsymbol{\theta}}\boldsymbol{\theta})]^T, \qquad (5)$$

where

$$G_{\boldsymbol{\varphi}_1} \in \mathbb{R}^{(l_p, 2)} \sim \mathcal{N}(\boldsymbol{\rho}_{\boldsymbol{\varphi}_1}, \boldsymbol{\Sigma}_{\boldsymbol{\varphi}_1}), \quad \gamma(\boldsymbol{\varphi}_1) \in \mathbb{R}^{2l_p}, \quad (6)$$

$$G_{\boldsymbol{\varphi}_2} \in \mathbb{R}^{(l_p, 2)} \sim \mathcal{N}(\boldsymbol{\rho}_{\boldsymbol{\varphi}_2}, \boldsymbol{\Sigma}_{\boldsymbol{\varphi}_2}), \quad \gamma(\boldsymbol{\varphi}_2) \in \mathbb{R}^{2l_p}, \quad (7)$$

$$G_{\boldsymbol{\theta}} \in \mathbb{R}^{(l_\theta, 2)} \sim \mathcal{N}(\boldsymbol{\rho}_{\boldsymbol{\theta}}, \boldsymbol{\Sigma}_{\boldsymbol{\theta}}) \quad \gamma(\boldsymbol{\theta}) \in \mathbb{R}^{2l_\theta}. \quad (8)$$

The l_p and l_θ are the lengths of the sampled Fourier basis frequencies. The $(\boldsymbol{\rho}_{\boldsymbol{\varphi}_1}, \boldsymbol{\rho}_{\boldsymbol{\varphi}_2}, \boldsymbol{\rho}_{\boldsymbol{\theta}})$ and $(\boldsymbol{\Sigma}_{\boldsymbol{\varphi}_1}, \boldsymbol{\Sigma}_{\boldsymbol{\varphi}_2}, \boldsymbol{\Sigma}_{\boldsymbol{\theta}})$ represent mean vectors and covariance matrices, respectively. To represent position information ($\gamma(\boldsymbol{\varphi}_1)$, $\gamma(\boldsymbol{\varphi}_2)$) and orientation information ($\gamma(\boldsymbol{\theta})$) in a unified representation space, we set $l_p = l_\theta$.

In many HBB prompt encoders of BSMs, $(\boldsymbol{\rho}_{\boldsymbol{\varphi}_1}, \boldsymbol{\rho}_{\boldsymbol{\varphi}_2}, \boldsymbol{\rho}_{\boldsymbol{\theta}})$ and $(\boldsymbol{\Sigma}_{\boldsymbol{\varphi}_1}, \boldsymbol{\Sigma}_{\boldsymbol{\varphi}_2}, \boldsymbol{\Sigma}_{\boldsymbol{\theta}})$ are considered as hyperparameters, which leads to difficulty in adapting to changes in datasets and searching optimal parameter settings. In CFNet, we adaptively learn $(\boldsymbol{\Sigma}_{\boldsymbol{\varphi}_1}, \boldsymbol{\Sigma}_{\boldsymbol{\varphi}_2}, \boldsymbol{\Sigma}_{\boldsymbol{\theta}})$. $(\boldsymbol{\rho}_{\boldsymbol{\varphi}_1}, \boldsymbol{\rho}_{\boldsymbol{\varphi}_2}, \boldsymbol{\rho}_{\boldsymbol{\theta}})$ are fixedly set to 0. Concretely, $(\boldsymbol{\Sigma}_{\boldsymbol{\varphi}_1}, \boldsymbol{\Sigma}_{\boldsymbol{\varphi}_2}, \boldsymbol{\Sigma}_{\boldsymbol{\theta}})$ are the weights of a learnable embedding layer.

Inspired by SAM, the mapped random Fourier features ($\gamma(\boldsymbol{\varphi}_1)$ and $\gamma(\boldsymbol{\varphi}_2)$) are summed with two learned embeddings ($\boldsymbol{\omega}_1$ and $\boldsymbol{\omega}_2$) that represent the top-left corner point and bottom-right corner point in CFNet, respectively.

$$\mathcal{E}(\boldsymbol{\varphi}_1) = \gamma(\boldsymbol{\varphi}_1) + \boldsymbol{\omega}_1, \qquad (9)$$

$$\mathcal{E}(\boldsymbol{\varphi}_2) = \gamma(\boldsymbol{\varphi}_2) + \boldsymbol{\omega}_2. \qquad (10)$$

Then, we obtain the encoded feature embeddings $\mathcal{E}(\boldsymbol{\varphi}_p)$ with respect to position information, which is given as

$$\mathcal{E}(\boldsymbol{\varphi}_p) = \text{Concat}[\mathcal{E}(\boldsymbol{\varphi}_1), \quad \mathcal{E}(\boldsymbol{\varphi}_2)]. \qquad (11)$$

On the other hand, the parameterized orientation representation ($\sin\theta, \cos\theta$) of an OBB suffers from the boundary discontinuity problem [25]. Due to the periodicity of orientations, at boundary orientations (such as $0°$ and $180°$), small changes in orientations will result in large jumps in ($\sin\theta, \cos\theta$). To alleviate the boundary discontinuity problem, CFNet introduces learnable orientation correction embeddings $\boldsymbol{\omega}_\theta$. At the orientations where the boundary dis-

continuity problem occurs, $\boldsymbol{\omega}_\theta$ adaptively adjusts the effect of this problem. Hence, the encoded feature embeddings $\mathcal{E}(\boldsymbol{\theta})$ with respect to orientation information are

$$\mathcal{E}(\boldsymbol{\theta}) = \gamma(\boldsymbol{\theta}) + \boldsymbol{\omega}_\theta. \qquad (12)$$

Finally, the encoded OBB prompt embeddings $\mathcal{P}_{\text{OBB}}$ (also called prompt embeddings) are the concatenation of the encoded position feature embeddings and encoded orientation feature embeddings, which is described as

$$\mathcal{P}_{\text{OBB}} = \text{Concat}[\mathcal{E}(\boldsymbol{\varphi}_p), \quad \mathcal{E}(\boldsymbol{\theta})]. \qquad (13)$$

C. Knowledge Distillation

BSMs exhibit powerful performance, however they usually have high computational complexity. Some methods, such as MobileSAM [19], focus on distilling image encoders. However, the performance gap between the distilled model and the teacher model is still large. To tackle this, CFNet uses the distilled image encoders, and further distills the prompt encoders and mask decoders of BSMs. Considering the powerful data-fitting capability of the teacher model, the student model only imitates the teacher model and does not learn from GT labels. Furthermore, to further enhance the performance and generalization capability of the student model, Gaussian smoothing is applied to teacher model outputs. The process of knowledge distillation for the proposed OBB prompt encoder and mask decoder is shown in Fig. 4.

We define a one-dimensional Gaussian kernel $\mathbf{G}_k^1(x_i; \sigma)$ with a length of k, which is given as

$$\mathbf{G}_k^1(x_i; \sigma) = \frac{1}{\mathbf{G}_s^1} e^{-[\frac{(x_i - x_c)^2}{2\sigma^2}]}, \qquad (14)$$

where

$$\mathbf{G}_s^1 = \sum_i e^{-[\frac{(x_i - x_c)^2}{2\sigma^2}]}, \quad i \in \{0, 1, \ldots, k-1\}. \qquad (15)$$

The x_i and x_c represent the position of each element and the central position, respectively. σ is the standard deviation. Given the encoded feature embeddings of the teacher model with respect to the top-left point ($\mathcal{E}^t(\boldsymbol{\varphi}_1) \in \mathbb{R}^{2l}$, $l = l_p = l_\theta$), bottom-right point ($\mathcal{E}^t(\boldsymbol{\varphi}_2) \in \mathbb{R}^{2l}$) and orientation ($\mathcal{E}^t(\boldsymbol{\theta}) \in \mathbb{R}^{2l}$), we perform Gaussian smoothing by convolving the

Gaussian kernel $\mathbf{G}_k^1$ with these encoded embeddings.

$$G^t(\boldsymbol{\varphi}_1) = \mathbf{G}_k^1 \circledast \mathcal{E}^t(\boldsymbol{\varphi}_1), \tag{16}$$

$$G^t(\boldsymbol{\varphi}_2) = \mathbf{G}_k^1 \circledast \mathcal{E}^t(\boldsymbol{\varphi}_2), \tag{17}$$

$$G^t(\boldsymbol{\theta}) = \mathbf{G}_k^1 \circledast \mathcal{E}^t(\boldsymbol{\theta}), \tag{18}$$

where $\circledast$ represents the convolution operation.

Then, the corresponding encoded feature embeddings $(\mathcal{E}^s(\boldsymbol{\varphi}_1), \mathcal{E}^s(\boldsymbol{\varphi}_2), \mathcal{E}^s(\boldsymbol{\theta}))$ of the student model mimic the smoothed feature embeddings $(G^t(\boldsymbol{\varphi}_1), G^t(\boldsymbol{\varphi}_2), G^t(\boldsymbol{\theta}))$ of the teacher model. The mean squared error (MSE) loss $(\mathcal{L}_{\text{prompt}})$ is used as the loss function.

$$\begin{aligned} \mathcal{L}_{\text{prompt}} = & \frac{1}{2l}||G^t(\boldsymbol{\varphi}_1) - \mathcal{E}^s(\boldsymbol{\varphi}_1)||_2^2 \\ & + \frac{1}{2l}||G^t(\boldsymbol{\varphi}_2) - \mathcal{E}^s(\boldsymbol{\varphi}_2)||_2^2 \\ & + \frac{1}{2l}||G^t(\boldsymbol{\theta}) - \mathcal{E}^s(\boldsymbol{\theta})||_2^2. \end{aligned} \tag{19}$$

For knowledge distillation on the mask decoder of a BSM, Gaussian smoothing makes the transition between boundary regions of different classes smoother and improves generalization capability. As the mask is two-dimensional, a two-dimensional Gaussian kernel $\mathbf{G}_{k \times k}^2(u_i, v_j; \delta)$ with a size of $k \times k$ is given as

$$\mathbf{G}_{k \times k}^2(u_i, v_j; \delta) = \frac{1}{\mathbf{G}_s^2} e^{-\left[\frac{(u_i - u_c)^2 + (v_j - v_c)^2}{2\delta^2}\right]}, \tag{20}$$

where

$$\mathbf{G}_s^2 = \sum_i \sum_j e^{-\left[\frac{(u_i - u_c)^2 + (v_j - v_c)^2}{2\delta^2}\right]}, \; i, j \in \{0, 1, \dots, k-1\}. \tag{21}$$

The (u_i, v_j) and (u_c, v_c) represent the position of each element and the central position, respectively. δ is the standard deviation. In knowledge distillation for segmentation tasks, unlike current methods [22], [24] that apply Gaussian smoothing to GT labels, we apply it to masks generated by the teacher model.

Since the detected OBBs distinguish instances and identify classes, the output mask is only responsible for distinguishing between foreground and background and has a shape of (H, W), where H and W represent the height and width of the input image, respectively. Given the output M^t of the mask decoder of the teacher model, we first use the sigmoid function $\sigma(\cdot)$ to generate a foreground probability map, and then convolve it with the Gaussian kernel $\mathbf{G}_{k \times k}^2$.

$$G(M^t) = \sigma(M^t) \circledast \mathbf{G}_{k \times k}^2, \tag{22}$$

Subsequently, the generated smoothed target $G(M^t)$ serves as the supervision target for the corresponding probability map $(\sigma(M^s))$ of the mask decoder of the student model. We use the binary cross entropy (BCE) loss $(\mathcal{L}_{\text{mask}})$ as the loss function, which is described as

$$\mathcal{L}_{\text{mask}} = -\frac{1}{HW} \sum_{m^t, m^s} [m^t \log m^s + (1 - m^t) \log(1 - m^s)],$$

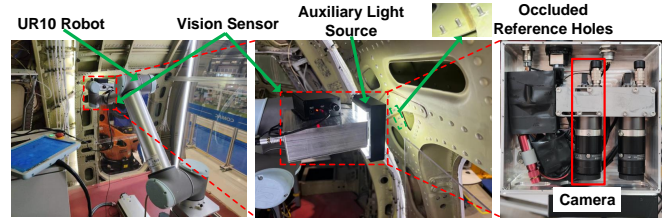$$m^t \in G(M^t), m^s \in \sigma(M^s). \tag{23}$$

Fig. 5. Self-designed robotic system for completely occluded object instance segmentation in the industrial robot assembly environment of the large commercial aircraft C919.

Hence, the final distillation loss $(\mathcal{L}_{\text{total}})$ is

$$\mathcal{L}_{\text{total}} = \lambda \cdot \mathcal{L}_{\text{prompt}} + (1 - \lambda) \cdot \mathcal{L}_{\text{mask}}, \tag{24}$$

where λ is the trade-off factor between the distillation loss of the OBB prompt encoder and that of the mask decoder.

IV. EXPERIMENTS

A. Dataset

To verify the effectiveness of the proposed methods, we conduct completely occluded object instance segmentation and dense object instance segmentation experiments on self-collected industrial and public datasets, respectively.

1) Industrial Dataset for Completely Occluded Objects: The self-designed industrial robotic vision system for large commercial aircraft assembly is shown in Fig. 5. It mainly consists of a UR10 robot, a vision sensor and a computer. Specifically, the UR10 robot is used to carry the vision sensor for operations. The computer is responsible for receiving and processing the image data collected by the vision sensor, and it runs the algorithm for completely occluded object instance segmentation. Due to the limited working space, reference holes are usually observed from the side.

All the images in the dataset are collected by this system, including three types of occluded reference holes, i.e., reference holes with bolts, nuts and untreated bolts (see the left image of Fig. 1). To reflect complex and changeable environments in the assembly process, each type of reference hole is photographed with the camera at various perspectives, distances and lighting conditions. We obtain a total of 800 images, with approximately the same number of each type. These images are divided into a training set, a validation set, and a testing set in a ratio of $7 : 1 : 2$ in a uniform sampling manner. All images are cropped to 1024×1024. Then, these images are first flipped horizontally and vertically to quadruple the number. Experimental GT labels are obtained from industrial standard workpieces. Furthermore, the Mosaic method that randomly mixes four images is used for data augmentation.

2) Public Dataset for Dense Objects: iSAID [8] is a large-scale and densely annotated instance segmentation dataset in aerial images. It has 655,451 object instances across 15 categories. The training set, validation set and testing set contain 1411, 458 and 937 images, respectively. All images are cropped into 1024×1024 patches with a stride of 500. Since iSAID dataset does not provide the GT parameters
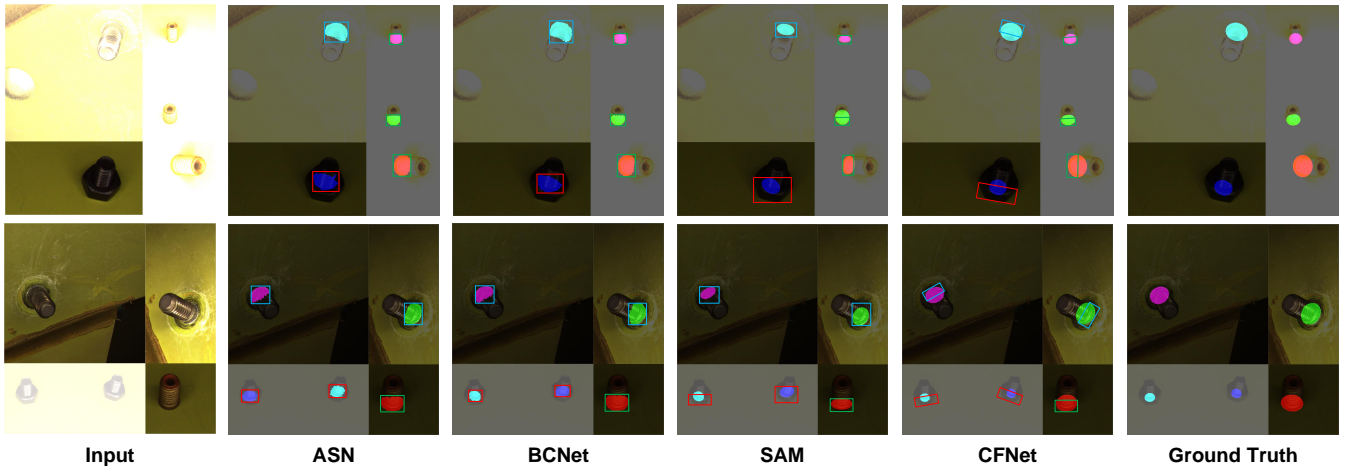
Fig. 6. Some visualization results on the completely occluded object instance segmentation dataset. Bounding boxes of different colors and segmentation masks of different colors represent different object classes and different instances, respectively.

of OBBs, the smallest OBBs of instance masks are used as regression targets. We only choose densely distributed large vehicles, small vehicles and ships as targets for dense object instance segmentation.

B. Implementation Details

The training settings for Oriented R-CNN [14] are the same as the original method. In the OBB prompt encoder, the length of the sampled Fourier basis frequencies is 128. For knowledge distillation, the teacher model (called CFNet*) is based on SAM with the powerful ViT (vision transformer)-H image encoder and the proposed OBB prompt encoder. The student model (i.e., CFNet) uses a lightweight pretrained ViT-Tiny image encoder and the proposed OBB prompt encoder. Their mask decoders and OBB detection modules are the same. During training, the weights of their image encoders are frozen, and the other parts are fine-tuned. The teacher model has the same training loss as SAM and has been trained before distillation. The trade-off factor λ for the distillation loss is 0.1. More implementation details can be found in our open-source code. All experiments are conducted on an RTX 3080Ti GPU. For evaluation, we use the standard COCO metrics: AP (i.e., AP_{50-95}), AP_{50} and AP_{75}, where "AP" means average precision over IoU (Intersection over Union) threshold.

C. Completely Occluded Object Instance Segmentation

In completely occluded object instance segmentation experiments, we compare CFNet, SAM, and amodal methods. SAM uses the ViT-H to encode images and the HBB detection branch of Mask R-CNN to generate HBB prompts (the same below). Amodal methods directly predict occludee instances. CFNet and SAM perform the proposed instance segmentation method on occluders to obtain occludee instances. We also include SAM after fine-tuning on this dataset and the teacher model (CFNet*) used for distillation in comparison. For fair comparison, we replace the backbones of current amodal instance segmentation methods with the ViT-H image encoder used in BSMs (indicated by †).

Method	AP	AP_{50}	AP_{75}	FPS
AmodalMask [15]	19.49	35.18	24.36	16.1
ASN [5]	40.88	61.24	45.93	18.6
ORCNN [6]	37.60	57.78	40.16	**22.2**
BCNet [4]	45.30	65.13	51.79	7.4
BCNet†	50.09	69.30	56.42	2.7
SAM [13]	26.15	42.74	30.28	2.8
Fine-tuned SAM	68.66	82.23	71.38	2.8
CFNet*	**75.13**	**89.21**	**77.98**	2.7
CFNet	73.46	86.48	76.20	20.4

As shown in Table I, the accuracy of CFNet and CFNet* is superior to other methods, especially for high-precision metrics. Additionally, CFNet exhibits competitive inference speed. Some visualization results are presented in Fig. 6. Compared with amodal instance segmentation methods, CFNet provides an effective solution for completely occluded object instance segmentation. In addition, compared with fine-tuned SAM using HBBs, the accuracy of CFNet and CFNet* using OBBs is significantly improved, which indicates the necessity of using OBBs. Moreover, our proposed knowledge distillation method significantly reduces the computational complexity with a minor loss in accuracy.

D. Dense Object Instance Segmentation

For dense object instance segmentation, we compare CFNet, SAM (with HBBs), and instance segmentation methods using OBBs. We also include fine-tuned SAM and the teacher model used for distillation in comparison, and replace the backbones of current instance segmentation methods using OBBs with the ViT-H image encoder used in BSMs.

As presented in Table II, CFNet and CFNet* outperform other methods, and CFNet achieves the highest inference speed of 20.4 FPS. In addition, CFNet achieves a remarkable dense object instance segmentation accuracy of 43.76% AP, 64.29% AP_{50}, and 46.13% AP_{75}. Fig. 7 shows some dense
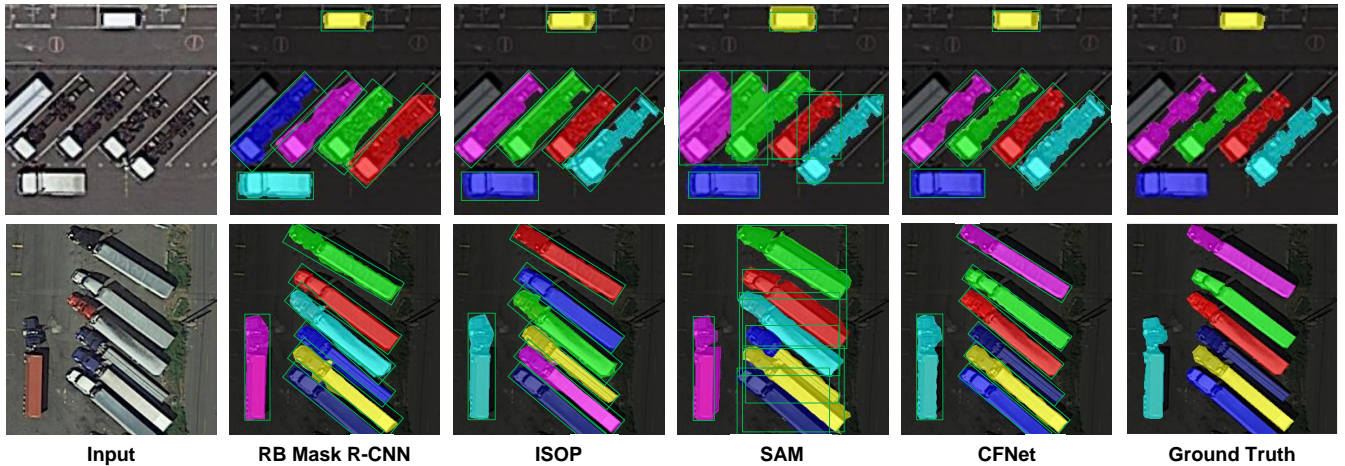
Fig. 7. Some visualization results on the dense object instance segmentation dataset iSAID. Bounding boxes of different colors and segmentation masks of different colors represent different object classes and different instances, respectively.

TABLE II

COMPARISON RESULTS ON THE DENSE OBJECT INSTANCE SEGMENTATION DATASET. "RB MASK R-CNN" REPRESENTS ROTATED BLEND MASK R-CNN [9].

Method	AP	AP_{50}	AP_{75}	FPS
OIS [10]	27.41	47.85	30.71	18.4
RB Mask R-CNN [9]	29.07	50.96	32.64	16.3
ISOP [12]	34.73	59.16	36.84	19.6
ISOP†	37.81	61.95	39.45	2.7
SAM [13]	14.37	41.88	18.52	2.8
Fine-tuned SAM	20.26	45.30	24.59	2.8
CFNet*	**45.10**	**66.45**	**47.92**	2.7
CFNet	43.76	64.29	46.13	**20.4**

TABLE III

PERFORMANCE OF EACH COMPONENT OF THE OBB PROMPT ENCODER.

GPE	AGPE	TCE+BCE	OCE	AP_{50}
✓				61.40
	✓			62.27
	✓	✓		63.56
	✓	✓	✓	**64.29**

TABLE IV

COMPARISON OF DIFFERENT LEARNING TARGETS AND LABEL SMOOTHING METHODS IN KNOWLEDGE DISTILLATION.

GT+ULS	GT+GS	T+GT	T	T+ULS	T+GS$^-$	T+GS
63.51	63.72	64.01	64.07	64.15	64.19	**64.24**

object instance segmentation results.

Compared with existing instance segmentation methods using OBBs, CFNet achieves higher accuracy since it reduces the dependence on OBBs and is based on BSMs. Significant accuracy improvements over fine-tuned SAM also indicate the benefit of using OBBs. Moreover, compared with CFNet*, the notable inference speed improvement and minor accuracy loss of CFNet also demonstrate the effectiveness of the proposed knowledge distillation method.

E. Ablation Studies

To evaluate the effectiveness of the components of CFNet, a series of ablation experiments are conducted on the iSAID dataset. We use the most commonly used AP_{50} as the metric.

1) Oriented Bounding Box Prompt Encoder: The OBB prompt encoder introduces positional encoding and specific embeddings to encode OBBs. In Table III, "OCE", "TCE" and "BCE" represent the specific orientation correction embeddings, top-left corner embeddings and bottom-right corner embeddings, respectively. Compared with GPE, AGPE encodes location information better by adaptively learning parameters of Gaussian distributions. Specific embeddings further improve instance segmentation performance.

2) Knowledge Distillation: We first compare the performance of CFNet learning from the teacher model and GT

labels, and test the impact of different label smoothing methods. "T" represents learning from the teacher model. The smoothing factor in ULS is 0.1. Gaussian smoothing (GS) has the same settings as SVLS, with a Gaussian kernel size of 3×3 and a standard deviation of 1.0. The weight factor of the teacher model and GT labels is 0.1. "GS$^-$" represents distillation only for the mask decoder.

The experimental results in Table IV demonstrate that learning from the teacher model has higher performance than learning from GT labels (learning only from GT labels means no knowledge distillation is performed), which is mainly thanks to the powerful data-fitting capabilities of BSMs. Furthermore, adding distillation for the OBB prompt encoder effectively enhances performance. Moreover, Gaussian smoothing further improves instance segmentation performance and is superior to ULS. In addition, we compare the impact of different parameter settings in Gaussian smoothing on instance segmentation performance in Table V. When $k = 5$, $\sigma = 0.3$, and $\delta = 1.0$, the highest instance segmentation accuracy of 64.29% AP_{50} is achieved.

3) Oriented Bounding Box Detection: To explore the impact of the OBB detection module on the instance segmentation performance, we compare Oriented R-CNN used

TABLE V

IMPACT OF PARAMETER SETTINGS IN GAUSSIAN SMOOTHING.

| | $\sigma = 0.3$ | | $\sigma = 0.5$ | |
	$\delta = 0.5$	$\delta = 1.0$	$\delta = 0.5$	$\delta = 1.0$
$k = 3$	64.24	64.24	64.20	64.17
$k = 5$	64.22	**64.29**	64.18	64.21
$k = 7$	64.19	64.25	64.15	64.14

TABLE VI

PERFORMANCE COMPARISON OF OBB AND HBB DETECTORS.

Mask R-CNN [16]	Oriented R-CNN [14]	Oriented Reppoints [26]	S2ANet [27]
42.95	64.29	**64.37**	64.06

in CFNet with some other OBB detection methods [26], [27]. In addition, a HBB detection method (HBB detection branch of Mask R-CNN) is also added for comparison. As shown in Table VI, the effective use of OBBs significantly improves instance segmentation accuracy, and CFNet is not sensitive to specific OBB detection methods.

V. CONCLUSIONS

This paper proposes CFNet, a unified coarse-to-fine framework for both completely occluded and dense object instance segmentation in robot vision measurement. CFNet uses BSMs and introduces a novel OBB prompt encoder. To make CFNet more lightweight, a knowledge distillation method involving Gaussian smoothing for teacher model outputs is applied to the OBB prompt encoder and mask decoder. Experiments on both industrial and public datasets demonstrate that CFNet outperforms current instance segmentation methods.

One limitation of this work is that CFNet relies on prior geometric properties to achieve completely occluded object instance segmentation. In the future, we plan to utilize more types of prior knowledge to improve the robustness. It is worth noting that CFNet not only uniformly handles the two difficulties of completely occluded and dense object instance segmentation, but also can be used for general instance segmentation tasks. Moreover, CFNet can also handle objects that are simultaneously in completely occluded and dense environments, such as instance segmentation of containers with UAVs. We also plan to explore more applications of CFNet in various complex robotic tasks.

REFERENCES

[1] Y. Liu, X. Chen, and P. Abbeel, "Self-supervised instance segmentation by grasping," in *IEEE Int. Conf. Intell. Robots Syst.*, 2023, pp. 1162–1169.

[2] Z. Dong, S. Liu, T. Zhou, H. Cheng, L. Zeng, X. Yu, and H. Liu, "Ppr-net:point-wise pose regression network for instance segmentation and 6d pose estimation in bin-picking scenarios," in *IEEE Int. Conf. Intell. Robots Syst.*, 2019, pp. 1773–1780.

[3] J. Mei, Y. Yang, M. Wang, X. Hou, L. Li, and Y. Liu, "Panet: Lidar panoptic segmentation with sparse instance proposal and aggregation," in *IEEE Int. Conf. Intell. Robots Syst.*, 2023, pp. 7726–7733.

[4] L. Ke, Y.-W. Tai, and C.-K. Tang, "Occlusion-aware instance segmentation via bilayer network architectures," *IEEE Trans. Pattern Anal. Mach. Intell.*, vol. 45, no. 8, pp. 10 197–10 211, 2023.

[5] L. Qi, L. Jiang, S. Liu, X. Shen, and J. Jia, "Amodal instance segmentation with kins dataset," in *IEEE Int. Conf. Comput. Vis. Pattern Recognit.*, June 2019.

[6] P. Follmann, R. König, P. Härtinger, M. Klostermann, and T. Böttger, "Learning to see the invisible: End-to-end trainable amodal instance segmentation," in *IEEE Winter Conf. Appl. Comput. Vis.*, 2019, pp. 1328–1336.

[7] K. Li and J. Malik, "Amodal instance segmentation," in *Eur. Conf. Comput. Vis.*, 2016, pp. 677–693.

[8] S. Waqas Zamir, A. Arora, A. Gupta, S. Khan, G. Sun, F. Shahbaz Khan, F. Zhu, L. Shao, G.-S. Xia, and X. Bai, "isaid: A large-scale dataset for instance segmentation in aerial images," in *IEEE Int. Conf. Comput. Vis. Pattern Recognit. Workshops*, June 2019.

[9] Z. Zhang and J. Du, "Accurate oriented instance segmentation in aerial images," in *Int. Conf. Image Graphics*, 2021, pp. 160–170.

[10] P. Follmann and R. König, "Oriented boxes for accurate instance segmentation," in *arXiv preprint arXiv:1911.07732*, 2020.

[11] Y. Feng, B. Yang, X. Li, C.-W. Fu, R. Cao, K. Chen, Q. Dou, M. Wei, Y.-H. Liu, and P.-A. Heng, "Towards robust part-aware instance segmentation for industrial bin picking," in *IEEE Int. Conf. Robot. Autom.*, 2022, pp. 405–411.

[12] T. Pan, J. Ding, J. Wang, W. Yang, and G.-S. Xia, "Instance segmentation with oriented proposals for aerial images," in *IEEE Int. Geosci. Remote Sens. symp.*, 2020, pp. 988–991.

[13] A. Kirillov, E. Mintun, N. Ravi, H. Mao, C. Rolland, L. Gustafson, T. Xiao, S. Whitehead, A. C. Berg, W.-Y. Lo, P. Dollar, and R. Girshick, "Segment anything," in *IEEE Int. Conf. Comput. Vis.*, October 2023, pp. 4015–4026.

[14] X. Xie, G. Cheng, J. Wang, X. Yao, and J. Han, "Oriented r-cnn for object detection," in *IEEE Int. Conf. Comput. Vis.*, October 2021, pp. 3520–3529.

[15] Y. Zhu, Y. Tian, D. Metaxas, and P. Dollar, "Semantic amodal segmentation," in *IEEE Int. Conf. Comput. Vis. Pattern Recognit.*, July 2017.

[16] K. He, G. Gkioxari, P. Dollar, and R. Girshick, "Mask r-cnn," in *IEEE Int. Conf. Comput. Vis.*, Oct 2017.

[17] F. Li, H. Zhang, H. Xu, S. Liu, L. Zhang, L. M. Ni, and H.-Y. Shum, "Mask dino: Towards a unified transformer-based framework for object detection and segmentation," in *IEEE Int. Conf. Comput. Vis. Pattern Recognit.*, June 2023, pp. 3041–3050.

[18] Y. Huang, X. Yang, L. Liu, H. Zhou, A. Chang, X. Zhou, R. Chen, J. Yu, J. Chen, C. Chen, S. Liu, H. Chi, X. Hu, K. Yue, L. Li, V. Grau, D.-P. Fan, F. Dong, and D. Ni, "Segment anything model for medical images?" *Med. Image Anal.*, vol. 92, p. 103061, 2024.

[19] C. Zhang, D. Han, Y. Qiao, J. U. Kim, S.-H. Bae, S. Lee, and C. S. Hong, "Faster segment anything: Towards lightweight sam for mobile applications," in *arXiv preprint arXiv:2306.14289*, 2023.

[20] M. Tancik, P. Srinivasan, B. Mildenhall, S. Fridovich-Keil, N. Raghavan, U. Singhal, R. Ramamoorthi, J. Barron, and R. Ng, "Fourier features let networks learn high frequency functions in low dimensional domains," in *Adv. Neural Inf. Process. Syst.*, vol. 33, 2020, pp. 7537–7547.

[21] C. Szegedy, V. Vanhoucke, S. Ioffe, J. Shlens, and Z. Wojna, "Rethinking the inception architecture for computer vision," in *IEEE Int. Conf. Comput. Vis. Pattern Recognit.*, June 2016.

[22] M. Islam and B. Glocker, "Spatially varying label smoothing: Capturing uncertainty from expert annotations," in *Inf. Process. Med. Imag.*, 2021, pp. 677–688.

[23] S. Park, J. Kim, and Y. S. Heo, "Semantic segmentation using pixel-wise adaptive label smoothing via self-knowledge distillation for limited labeling data," *Sensors*, vol. 22, no. 7, 2022.

[24] M. Islam, L. Seenivasan, S. P. Sharan, V. K. Viekash, B. Gupta, B. Glocker, and H. Ren, "Paced-curriculum distillation with prediction and label uncertainty for image segmentation," in *Int. J. Comput. Assisted Radiology surg.*, vol. 18, 2023, pp. 1875–1883.

[25] X. Yang, G. Zhang, X. Yang, Y. Zhou, W. Wang, J. Tang, T. He, and J. Yan, "Detecting rotated objects as gaussian distributions and its 3-d generalization," *IEEE Trans. Pattern Anal. Mach. Intell.*, vol. 45, no. 4, pp. 4335–4354, 2023.

[26] W. Li, Y. Chen, K. Hu, and J. Zhu, "Oriented reppoints for aerial object detection," in *IEEE Int. Conf. Comput. Vis. Pattern Recognit.*, June 2022, pp. 1829–1838.

[27] J. Han, J. Ding, J. Li, and G.-S. Xia, "Align deep features for oriented object detection," *IEEE Trans. Geosci. Remote Sens.*, vol. 60, pp. 1–11, 2022.